Int. J. Heat Mass Transfer. Vol. 29, No. 2, pp. 183–192, 1986
Printed in Great Britain

0017–9310/86 $3.00 + 0.00

Natural-convection-dominated melting heat transfer in an inclined rectangular enclosure

B. W. WEBB and R. VISKANTA
School of Mechanical Engineering, Purdue University, West Lafayette, IN 47907, U.S.A.

(*Received* 22 *April* 1985 *and in final form* 30 *July* 1985)

Abstract—Melting heat transfer in an inclined rectangular enclosure is investigated experimentally. The effect of enclosure inclination is to establish three-dimensional natural convective motion which intensifies as the inclination angle from the vertical is increased. The three-dimensionality of the flow field results in nonuniform melting of the solid. The interface morphology is used to infer flow structure and the extent of three-dimensional energy transport. These flow patterns are found to be dependent on the angle of inclination and the initial solid subcooling. A correlation is presented describing the effect of inclination angle on the timewise variation of the melt fraction. A one-dimensional theoretical model is outlined and predictions are compared to experimental data.

INTRODUCTION

MELTING and solidification are important problems of current technological interest. The concern with phase-change problems is motivated by latent heat-of-fusion energy storage applications, as well as crystal growth and materials processing relevance. A recent survey of the literature and a comprehensive discussion of the complexities associated with general melting/solidification heat transfer problems is available [1].

In traditional analytical approaches to the problem of melting of a phase-change material (PCM) in contact with a heated wall, it was assumed that conduction was the sole means of energy transport across the liquid layer. Investigations have shown, however, that natural convection in the melt region can play a major role in the heat transfer process [2, 3]. A recent review summarizes the extent of natural convection dominance in phase-change systems [4]. In brief, the role of natural convection in melting heat transfer is to significantly increase the melting rate over that produced in conduction-dominated systems.

Most of the work (both experimental and numerical) treating the effect of natural convection in enclosures has dealt with vertical systems with one wall heated to a temperature above the fusion point of the PCM. Under these conditions the hydrodynamic and thermal fields in the melt region can be approximated as being two-dimensional. Liquid PCM is heated and rises along the heat source wall, then descends along the solid–liquid interface, melting solid material as it descends. Since the temperature of the liquid PCM is highest near the top of the natural convection zone, more melting occurs there, resulting in an elongated melt cavity that expands with time. The recirculating flow is stable and well characterized.

A recent experimental study [5] has presented the results of the effect of melting a solid PCM from below. The resulting thermally unstable flow field yielded Bénard-like convection cells. These cells were manifested in the solid–liquid interface by hexagonal, hemispherically-capped domes where high-temperature rising fluid increased the local melting rate. The flow was strongly three-dimensional, resulting in effective heat transport from the hot bottom to the solid–liquid interface.

To date, it appears that there have been no experimental studies treating natural-convection-dominated heat transfer in inclined enclosures. Melting in inclined enclosures is expected to reveal complex flow and thermal fields deviating from the 'boundary-layer' regime melting heat transfer found in two-dimensional recirculating flow melting systems described above. Higher melting rates are anticipated as the natural convection flow patterns in the melt region reach some combination of the two-dimensional melting from a hot vertical wall and the strongly three-dimensional flow found in melting of a solid from below. Obviously, the type of flow pattern found will be strongly dependent on the inclination angle of the enclosure.

The work to be described here appears to be the first experimental study investigating natural-convection-dominated melting heat transfer in an inclined rectangular enclosure. A one-dimensional melting model based on Nusselt number correlations for inclined rectangular enclosures in the absence of phase change is developed and predictions are compared with experimental results.

EXPERIMENTS

Test apparatus

The experimental test cell consisted of a Plexiglass frame inside which a copper heat exchanger was situated, forming one of the vertical walls. Provision was made for injection of dyed paraffin into the test cell for visualizing the flow structure. The front and back

NOMENCLATURE

A	aspect ratio of cavity, H/W
c	specific heat
D	depth of phase-change material normal to x–y plane
f	molten volume fraction, V_l/V_{tot}
Fo	Fourier number, $\alpha_l t/H^2$
$\bar{h}$	average heat transfer coefficient, equation (8)
Δh_f	latent heat of fusion
H	initial height of phase-change material in y-direction
k	thermal conductivity
k^*	thermal conductivity ratio, k_s/k_l
Nu	Nusselt number, hH/k_l
Pr	Prandtl number, ν/α
Q_{tot}	total heat input to system
Ra	Rayleigh number, $g\beta(T_h - T_f)H^3/\nu\alpha_l$
s	location of melting front, $s(y, t)$
$\bar{s}$	average interface position
s^*	dimensionless interface position, s/H
Ste	Stefan number, $c_l(T_h - T_f)/\Delta h_f$
S_c	subcooling parameter, $c_s(T_f - T_i)/\Delta h_f$
t	time
T	temperature
T_f	fusion temperature
T_h	temperature of heated wall
T_i	initial temperature of solid
v_n	local normal interface velocity
v_n^*	dimensionless interface velocity, $v_n H/\alpha_l$
V	volume
W	width of cavity in x-direction
x	coordinate direction normal to heated wall
y	coordinate direction parallel to heated wall
y^*	dimensionless coordinate, y/H.

Greek symbols

α	thermal diffusivity
α^*	thermal diffusivity ratio, α_s/α_l
θ	dimensionless temperature, $(T - T_f)/(T_h - T_f)$
ν	kinematic viscosity
ρ	density
ρ^*	density ratio, ρ_s/ρ_l
τ	dimensionless time, $Fo\ Ste$
ψ	inclination angle measured from vertical.

Subscripts

l	refers to liquid phase
s	refers to solid phase.

walls of the test cell were optical quality glass, permitting visual observation of the flow patterns and of the solid–liquid interface motion. The fourth vertical side wall was designed so as to be readily removable. This provided the capability of removing the remaining solid PCM block at any time during the experiment. When fully assembled the interior dimensions of the test cell were 25.4 × 6.35 × 4.06 cm deep. The unmelted solid PCM adhered to the walls of the test cell, preventing it from falling against the heat exchanger. This permitted study of the effect of inclination on natural-convection-dominated melting rather than direct-contact melting. The height of the cell was sufficient to provide ample room for PCM expansion upon melting, particularly at higher inclination angles. The top boundary condition was thus one of a horizontal free surface (Fig. 1). Once assembled the entire cell, including top and bottom, was covered with 5 cm of styrofoam insulation.

The temperature of the side-wall heat exchanger was maintained by circulating a water–ethylene glycol solution from a constant temperature bath through its milled channels. In an effort to maintain uniformity of surface temperature the heat exchanger was fabricated in a counterflow scheme with milled inlet and outlet channels always running adjacent to each other. A single thermocouple inserted through the back of the heat exchanger was positioned near the wetted surface in order to measure the heated wall temperature. Thermocouples located inside the inlet and outlet tubes of the heat exchanger provided a measure of the temperature uniformity over the heated surface. It was

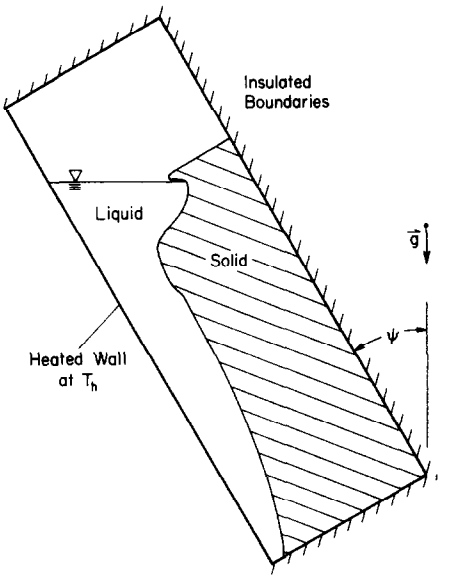

FIG. 1. Experimental test configuration and pertinent geometric parameters.

found that after the start of the experiment the heat exchanger required 3–4 min to reach the desired temperature. During this initial transient the inlet and outlet temperatures differed by 0.3–0.4°C. Monitored temperatures later in the experiment showed virtually no temperature drop across the heat exchanger. In addition, the heated surface temperature and the inlet and outlet temperatures agreed to within 0.1°C after the initial transient. Since the experiments typically required 2–3 h, the effect of the initial transient period on the reported results is deemed to be negligible. An incandescent light bulb and diffuser provided suitable background light for photographic recording of the solid–liquid interface position. A transparent grid on one of the front glass walls was used as a reference for later reconstruction of the solid–liquid interface contours.

Test procedure and data reduction

Research grade (99% pure) *n*-octadecane was used in all experiments. This material was selected because (1) it has a fusion temperature near ambient (27.4°C), advantageous in reducing heat losses to the ambient; (2) its liquid phase is transparent to visible radiation, allowing flow visualization and photographic observation of the system; and (3) the thermophysical properties of *n*-octadecane are reasonably well established.

The PCM was degasified in preparation for each experiment. This was necessary because absorbed gases, liberated at the solid–liquid interface and drawn to the surface by buoyancy, disturb the hydrodynamic and thermal fields in the melt. The degasification was accomplished by heating the PCM to a temperature well above its fusion point for approx. 1 h while drawing a vacuum on the containing flask. Still under vacuum, the flask was then immersed in ice and cooled quickly to a temperature near the fusion point, requiring about 2–3 h. The degasified liquid was then carefully syphoned into the test cell after which the entire assembly was immersed in an ice bath for solidification.

Since the solid/liquid density ratio of *n*-octadecane is greater than unity, the possibility exists for the formation of a concave upper surface on the PCM as it solidifies and contracts. This problem was circumvented by adding successively smaller amounts of liquid PCM to the test cell as it solidified. Additionally, formation of internal voids in the solid was prevented by irradiating the upper surface of the liquid PCM with a small lamp to ensure that solidification proceeded from the bottom up. After solidification, slight irregularities in the top surface were eliminated by quickly melting it with heated air, then allowing the resulting melt to soldify forming a planar surface. After solidification, the temperature of the fluid circulating in the heat exchanger was set at the desired value of initial subcooling. A uniform initial temperature in the solid was ensured by allowing it to equilibrate for a period of over 16 h.

After reaching solid temperature equilibrium, the test cell was oriented at the desired inclination angle. The melting experiments were then begun by impulsively circulating heated fluid through the heat exchanger. Direct injection of dyed paraffin into the liquid, and fish scales previously solidified in the PCM were used as flow visualization techniques. Attempts to record photographically the flow structure proved unsuccessful in the inclined experiments due to the strong three-dimensional motion in the melt region.

The solid–liquid interface position was recorded at preselected time intervals with a Nikon FE 35-mm camera. The contours of the solid–liquid interface position were reconstructed from the photographs, and the area of the unmelted solid was determined using a planimeter. This method of determining the molten volume was selected rather than direct weighing of the unmelted solid at predetermined time intervals during the experiment. Direct weighing would have required that the same experiment be repeated several times, with the obvious difficulty of ensuring identical initial and boundary conditions. In addition, the time required for sample preparation and thermal equilibration makes the direct weighing approach prohibitive. Since the flow field and resulting solid–liquid interface were three-dimensional the uncertainty in the planimeter-determined molten fraction was estimated to be about $\pm 10\%$. The measured weight of the final unmelted portion of the PCM for several experiments provided the basis for this estimate.

At the conclusion of each experiment the liquid was quickly syphoned off, and the unmelted portion of the PCM was removed by disassembling the fourth vertical side wall. The unmelted solid block was covered entirely with aluminum foil, ensuring that all ridges and grooves in the solid–liquid interface were well-represented. The aluminum-covered block was then spray-painted black and photographed, using side lighting to best illustrate the solid–liquid interface morphology. These photographs were used to qualitatively infer the flow structure in the melt. Finally, the test cell was thoroughly cleaned in preparation for another experiment.

MELTING CHARACTERISTICS

Interface contours

Solid–liquid interface contours were reconstructed from the photographs taken at selected time intervals during the experiments. Since the flow field was three-dimensional, the solid–liquid interface displayed three-dimensional characteristics. The contours shown, then, represent a silhouette of the maximum solid protrusion into the melt region. As mentioned previously, the liquid PCM was allowed to expand and form a free surface at the top of the test cell. The extension of the horizontal liquid free surface along the heat exchanger wall is not shown on the contours.

The melt contours for the vertical base case ($\psi = 0°$) are shown in Fig. 2(a). The interface motion is typical of those found in other vertical-wall melting studies. Early

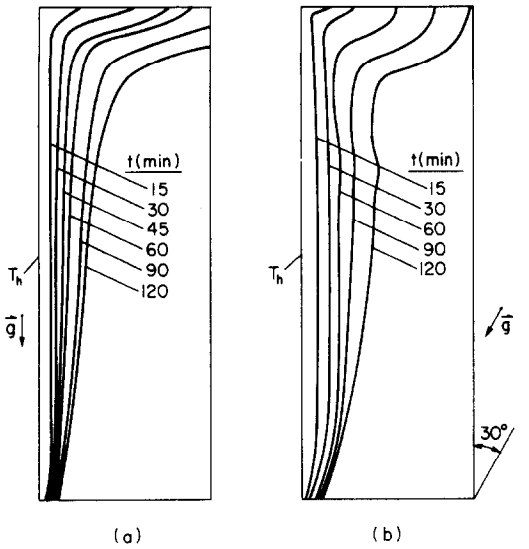

FIG. 2. Solid–liquid interface contours for $Ste = 0.105$, $S_c = 0.08$: (a) $\psi = 0°$, (b) $\psi = 30°$.

in the melting process the interface motion is uniform across the height of the cavity indicating a conduction-dominated melting regime. The slight curvature found at the top of the interface at early times is probably due to PCM expansion upon melting. The onset of natural convection corresponds reasonably well with published correlations [6, 7] detailing the dimensionless average gap width for transition from conduction. Higher melting rates are seen at the top of the cavity where the liquid PCM, having risen along the heat exchanger at the opposite wall, is at a higher temperature. Flow visualization using fish scales as a tracing technique revealed the conventional 'boundary-layer' regime with steep velocity gradients at the solid surfaces and a relatively stagnant core in the center. The melting rate was very low at the bottom of the cavity where the liquid was relatively cold. The flow was mainly two-dimensional with the only deviations being confined to a region approx. 0.5–0.75 cm from the front and back vertical walls.

Figure 2(b) illustrates the solid–liquid interface motion for the $\psi = 30°$ test case. The transition from conduction-dominated to natural-convection-dominated melting apparently occurs earlier, as evidenced by the slight concavity in the solid–liquid interface at $t = 15$ min. Comparison of these contours with those of Fig. 2(a) reveals higher curvature of the interface near the bottom. The deviations in the interface movement at the top of the cavity for the $\psi = 0°$ and $\psi = 30°$ cases are due mainly to the establishment of a horizontal free surface in the inclined study. The flow was three-dimensional: liquid PCM is heated at the hot wall, and rather than rising parallel to the heat exchanger as in the vertical test case, it rises vertically away from the wall. This accounts for the higher interface curvature near the bottom. An attempt to visualize the flow structure by injection of dyed paraffin revealed rapid dispersion, making it impossible to record photographically. As will be shown later, the strong three-dimensional flow is responsible for unusual and nonuniform melting at the solid–liquid interface.

An inflection point near $y^* = 2/3$ in the contours appears in Fig. 2(b) at approx. $t = 60$ min and is accentuated by time. It is at this point that fluid rising in a helical vortex from the heat exchanger meets liquid falling from the top of the melt cavity. Photographs of the interface presented later bear this out. Finally, the increased global melting rate increase is obvious for $\psi = 30°$.

The interface contours for $\psi = 60°$, $S_c = 0.08$ shown in Fig. 3(a) reveal a radical departure from those of the vertical base case. The melt front motion is more uniform across the height of the cavity. Very strong curvature at the bottom of the cavity again reveals hot fluid lifting from the heat exchanger towards the interface where high melting occurs. The boundary-layer regime seen in the vertical heat exchanger orientation is virtually nonexistent when $\psi = 60°$. Ridges and valleys in the contours intensify as time progresses and illustrate the strong three-dimensional nature of the flow. Again, the irregularity in the contours at the top is a result of the formation of the horizontal free surface there.

Figure 3(b) presents the contours for the same conditions as those found in Fig. 3(a) ($\psi = 60°$, $Ste = 0.105$) only with negligible subcooling ($S_c = 0.0018$). The results display qualitatively the same characteristics as the experiment with $S_c = 0.08$. The interface is slightly less irregular for $S_c = 0.0018$ and, as will be shown later, the flow patterns are somewhat different. As expected, a slightly higher melting rate is experienced when subcooling is negligible.

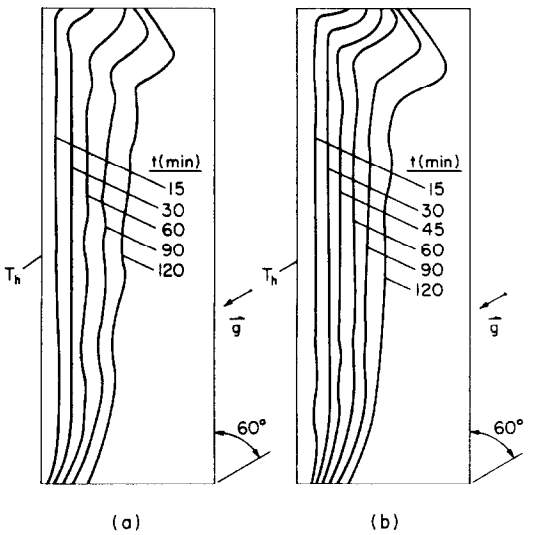

FIG. 3. Solid–liquid interface contours for $Ste = 0.105$, $\psi = 60°$: (a) $S_c = 0.08$, (b) $S_c = 0.0018$.

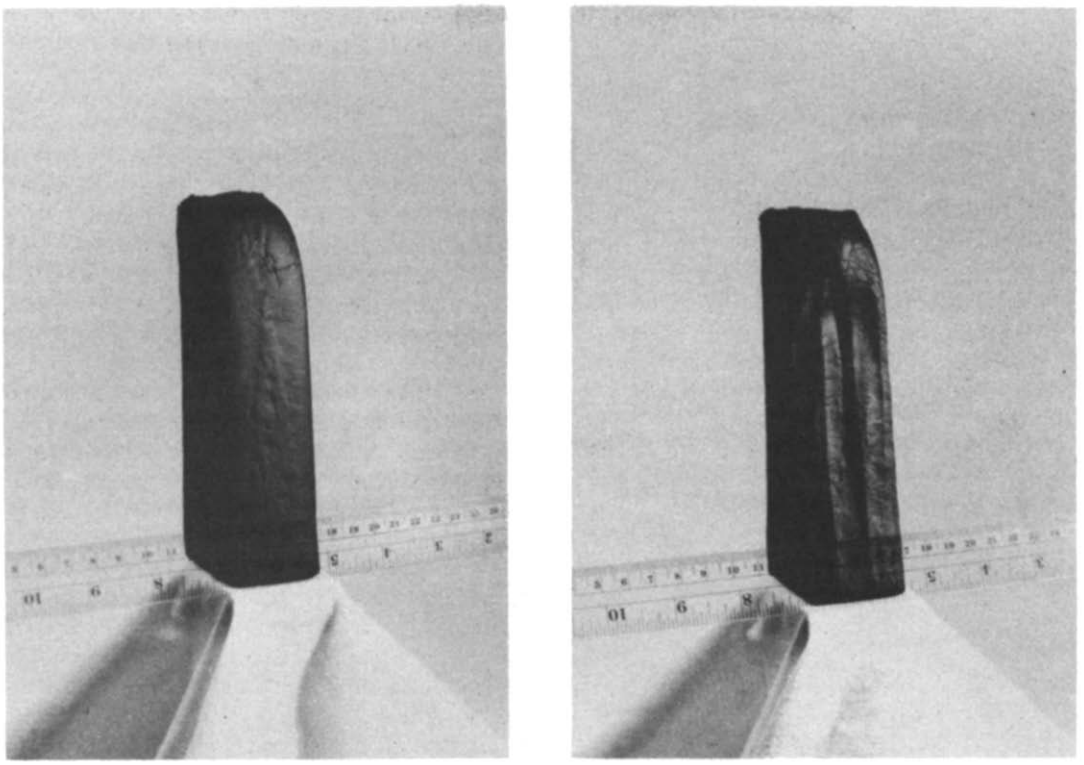

(a) (b)

FIG. 4. Solid–liquid interface morphology at $t = 135$ min for $Ste = 0.105$, $S_c = 0.08$: (a) $\psi = 0°$, (b) $\psi = 30°$.

Interface morphology

At the conclusion of each experiment the vertical side wall was disassembled and the remaining portion of unmelted solid PCM was removed. Each experiment was terminated at the same time so that the solid–liquid interface morphology could be compared and contrasted. The resulting photographs are shown in Figs. 4 and 5.

Figure 4(a) shows the interface for the vertical base case experiment. The interface is largely two-dimensional with the only deviations arising from conduction along the vertical front and back glass walls, which have a thermal conductivity substantially higher than that of *n*-octadecane.

Figure 4(b) illustrates the result of three-dimensional melting for $\psi = 30°$. Attention is drawn to the three distinct grooves along the length of the block. A regular pattern of helical flow can be inferred from fluid rising vertically away from the heat exchanger and impinging against the interface in regions of high melting, then cooling and falling back to the hot wall. The axis of the helical motion for the grooves in the interface is parallel to the interface itself. These helical flow patterns have been observed and predicted for natural convection in inclined rectangular enclosures in the absence of phase change [8, 9].

At an inclination angle of 60° [Fig. 5(a)] the grooves running the length of the block have been replaced by ridges and grooves running transverse to the vertical upslope. These irregularities are the result of near-cellular motion of the liquid in the melt region. The flow displays some vortex motion whose axis is now normal to the front and back walls. The helical motions parallel to the interface ($\psi = 30°$) merge and form a more cellular structure ($\psi = 60°$) as the inclination angle is increased. Finally, for a horizontal melting system the fully cellular hexagonal Bénard convection regime would be established resulting in the domed solid–liquid interface morphology discussed previously [5]. It is this strong three-dimensional motion and subsequently higher energy transport that is responsible for the higher and more uniform melting rate seen in the contours of Fig. 3(a).

Figure 5(b) offers a comparison with Fig. 5(a) as to the effect of initial solid subcooling on the flow field in the liquid PCM. The solid block in Fig. 5(b) ($\psi = 60°$, $S_c = 0.0018$) shows some similarity with the interface morphology found in Fig. 4(b) ($\psi = 30°, S_c = 0.08$). The ridges and grooves running parallel to the upslope for $S_c = 0.0018$ appear to be more dominant than the more cellular patterns found for $S_c = 0.08$ in the $\psi = 60°$ inclination experiments. This suggests that initial solid subcooling reinforces the tendency toward cellular natural convective motion in the melt. This conclusion is supported by findings [5] where the solid–liquid interface morphology was investigated in melting of a

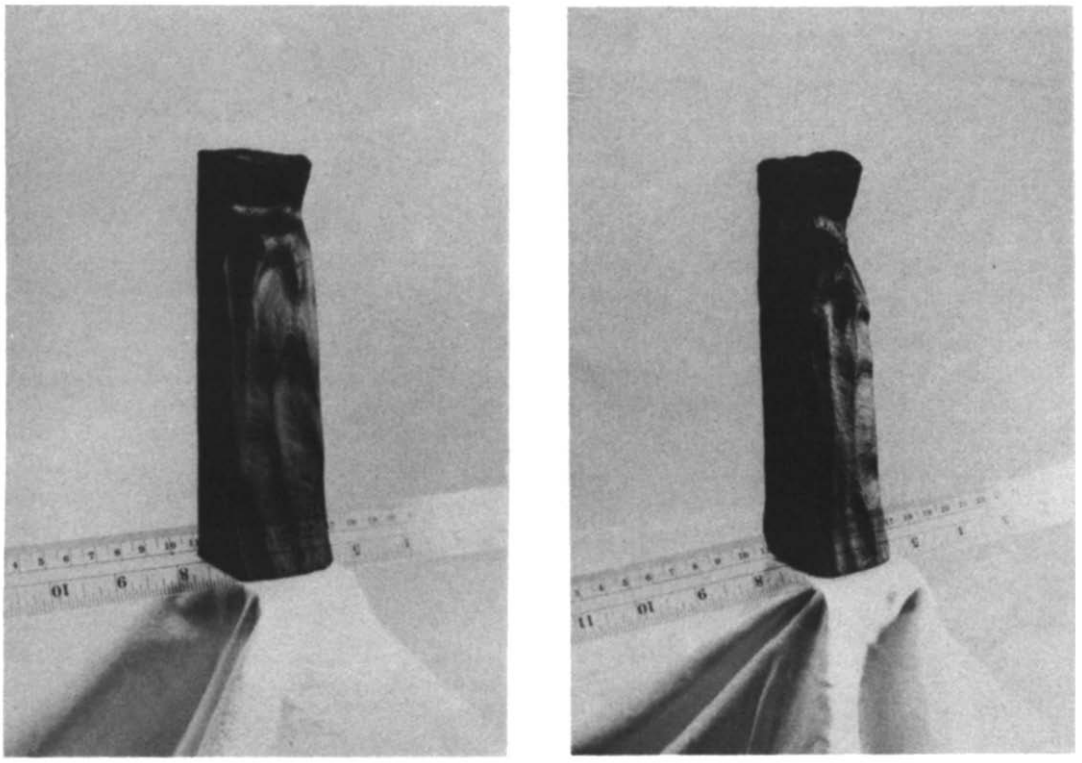

(a) (b)

FIG. 5. Solid–liquid interface morphology at $t = 135$ min for $Ste = 0.105$, $\psi = 60°$: (a) $S_c = 0.08$, (b) $S_c = 0.0018$.

PCM from below. It was found that the number of domes per unit projected area in the solid–liquid interface (formed by Bénard convection cells) increased with initial subcooling of the solid. Despite the loss of the more effective energy transport afforded by the cellular convective motion the melting rate is still higher when the initial subcooling is negligible.

Melting rate

Figure 6 presents the melting results for the inclination angles studied. The results (for initial subcooling $S_c = 0.08$) were correlated by the equation

$$f = 35.4\tau^{0.77} \cos\psi^{-0.4}. \quad (1)$$

Inclination of the initially solid PCM enhances the melting rate due to the onset of three-dimensional natural convection in the melt. The dependence on inclination angle is quite strong with an exponent of -0.4. The melt fraction for $\psi = 60°$ can be as large as 35% higher than that of the vertical base case. The correlation is only valid in the natural convection-dominated melting regime, since melting by pure conduction yields a melt fraction proportional to $\tau^{1/2}$. The duration of conduction-dominated melting was typically 5–10 min of the total melting time of 120 min.

Also included in the graph is the theoretical line describing purely conduction-dominated melting, obtained from an energy balance at the heated wall

$$f = A[2\tau/\rho^*(1 + S_c + Ste/2)]^{1/2}. \quad (2)$$

The effect of initial subcooling has been approximated in the derivation of this relation by assuming that the energy transferred to the solid–liquid interface must first supply the sensible heat in raising the solid

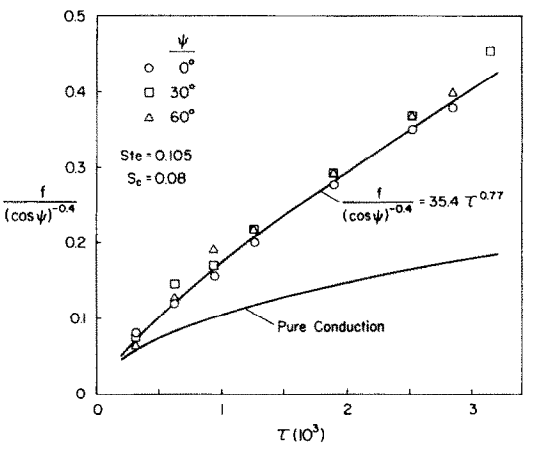

FIG. 6. Correlation of molten fraction–dimensionless time data.

temperature from its initial value T_i to the fusion point T_f. The remaining energy serves to supply latent heat for melting. All inclination angles offer a clear advantage over the pure conduction melting in terms of enhanced melting rate. The molten volume fraction is radically different especially at large times as the natural convective motion intensifies. It may also be concluded that the onset of natural convection in the melt occurs sooner as the inclination angle increases.

ONE-DIMENSIONAL MODEL

Analysis of melting from a heated vertical wall by solving the conservation equations of mass, momentum and energy in the melt and the energy equation in the solid is still under development. Numerical models outlined recently for two-dimensional melting [7, 10, 11] are very costly and require a fine grid near the solid boundaries in order to resolve accurately the high gradients there. This is critical in the prediction of the solid–liquid interface motion. The immobilization of the moving boundary still poses a considerable challenge. The added complexity of three-dimensional natural convection makes this type of approach prohibitive with current numerical algorithms and computer capabilities. A simple one-dimensional model was therefore formulated in an effort to predict the overall heat transfer and subsequent global melting rate.

The local energy balance at the solid–liquid interface yields

$$-k_l \nabla T \cdot \bar{n} = \rho_s \Delta h_f v_n - k_s \nabla T_s \cdot \bar{n} \tag{3}$$

where $\bar{n}$ is the unit vector normal to the interface in the direction of the solid region, and v_n is the local interface velocity in the direction of $\bar{n}$. In dimensionless form, then, the local interface velocity is governed by

$$v_n^* = \frac{Ste}{\rho^*}(k^* \nabla \theta_s \cdot \bar{n} - \nabla \theta \cdot \bar{n}) \tag{4}$$

where $-\nabla\theta \cdot \bar{n}$ may be replaced by the local Nusselt number Nu. If one assumes that on the average the solid–liquid interface remains planar, the average interface motion can be expressed as

$$v_n^* = Ste\left(\frac{\overline{Nu}}{\rho^*}\right) - \frac{\alpha^* S_c}{[(1/A) - s^*]} \tag{5}$$

or, in terms of the molten fraction

$$\frac{df}{d\tau} = A\left[\frac{\overline{Nu}}{\rho^*} - \frac{\alpha^* S_c}{Ste}\frac{A}{(1-f)}\right]. \tag{6}$$

Under the assumption of planar interface motion the liquid region becomes nothing more than a rectangular cavity. Consequently, the average Nusselt number can be obtained from published correlations for natural convection heat transfer in inclined rectangular enclosures. Such correlations are available in terms of the characteristic dimensionless parameters Ra, Pr, A and the inclination angle ψ [12].

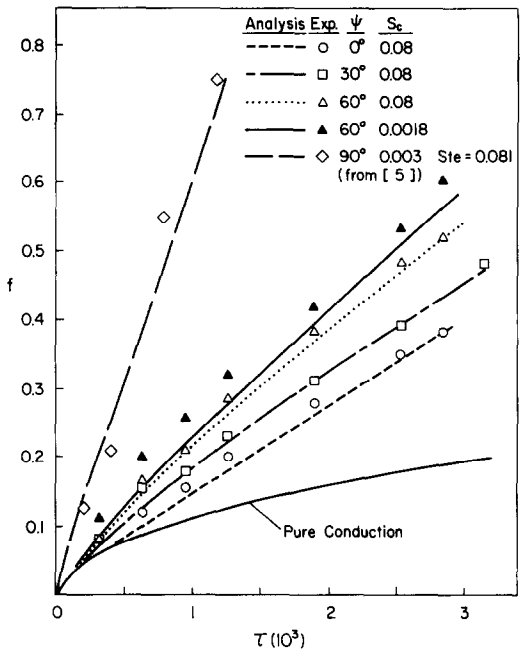

FIG. 7. Variation of molten fraction with dimensionless time.

The foregoing one-dimensional model for predicting the timewise variation of the molten fraction was implemented. Predictions were initialized using the pure conduction solution given by equation (2). Equation (6) was then integrated numerically, advancing the melt front in time explicitly. At early times when the melt gap was very small a Nusselt number of unity was used at each time step consistent with conduction-dominated melting. Later, as the melt region expanded the Nusselt number was determined from correlations [12] where the Rayleigh number and aspect ratio were calculated based on the instantaneous average width of the rectangular region. The computations were terminated when a preselected dimensionless time was reached.

Comparison of predictions based on the one-dimensional model presented in the foregoing and experimental data are shown in Fig. 7. There is good agreement; the average error between the two is about 9%. The effect of initial solid subcooling appears to be slightly less pronounced in the theoretical predictions than in the experimental results. This can probably be attributed to the one-dimensional nature of the model. The model underpredicts the molten volume fraction as a general rule. It may then be suggested that the effect of the free surface formation and interface curvature is to enhance somewhat the melting, since the model is based on a planar interface with correlations for natural convection in rectangular enclosures in the absence of phase change. Based on the parameters given [5], the model predicts quite well the timewise melt fraction advancement in a horizontal slab heated from below. The average error of 9% is definitely within the expected uncertainty of the experimental data, and the simple

one-dimensional model can therefore be used with some confidence in predicting the global melting rates of inclined solids.

HEAT TRANSFER

Heat transfer results can be inferred from the melt fraction versus time data presented previously. One can define a time-dependent spatially- and temporally-averaged Nusselt number

$$\tilde{Nu} = \frac{\tilde{h}H}{k_l} \tag{7}$$

where

$$\tilde{h} = \frac{Q_{tot}/t}{HD(T_h - T_f)}. \tag{8}$$

The average heat transfer coefficient defined in equation (8) is based on the total energy input to the system Q_{tot} over the total elapsed time since the onset of melting, t. The total heat input can be expressed as [13]

$$Q_{tot} = \int_{V_s} \rho_s c_s (T - T_i)\, dV_s + \int_{V_l} \rho_l c_l (T - T_f)\, dV_l + \rho_l V_l \Delta h_f. \tag{9}$$

Assuming that the average temperature of the liquid PCM is $(T_h + T_f)/2$, and similarly, that the average temperature of the unmelted solid PCM is $(T_f + T_i)/2$ the average Nusselt number can be expressed as

$$\tilde{Nu} = \frac{1}{A\tau}[f(1 + Ste/2) + \rho^* S_c(1 - f)/2]. \tag{10}$$

This average Nusselt number can then be determined from the instantaneous melt fraction data and the parameters of the system and experiment. The results are presented graphically in Fig. 8, where the average Nusselt number for each experiment is plotted as a function of dimensionless time τ. The $\tilde{Nu}$ vs τ behavior for inclined layers is similar to that of the vertical case, starting very high at early times. Its magnitude then decreases, approaching a quasi-steady value at later times when melting is dominated by natural convection. The results show clearly that the average Nusselt number increases with increasing angle of inclination. Again this is the result of strong three-dimensional convective motions which are intensified as the inclination angle increases.

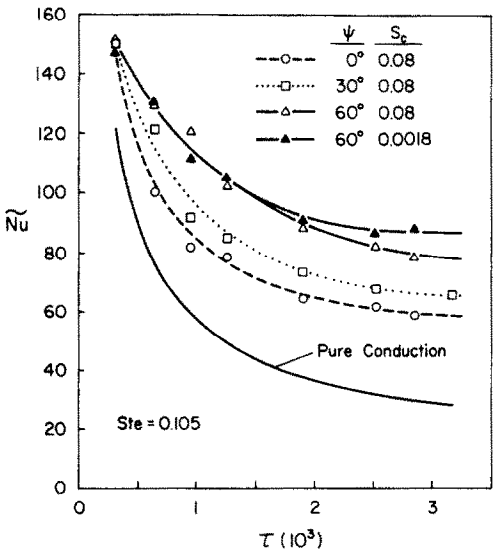

FIG. 8. Variation of spatially- and temporally-averaged Nusselt number with dimensionless time.

The $\tilde{Nu}$ vs τ behavior shows no local minimum as has been predicted theoretically for phase-change problems in vertical rectangular [7, 10, 11], vertical cylindrical [14] and horizontal cylindrical [15] geometries. This may be the result of the temporal averaging of the Nusselt number. It may also be conjectured that the local minimum in the temporal variation of the average Nusselt number is suppressed in the inclined melting system since natural convection is apparently dominant much earlier in the melting process. Note also that the average Nusselt number for pure conduction, determined by substitution of equation (2) in equation (10), is significantly lower than the experimental values shown.

The initial subcooling ($S_c = 0.08$) and negligible subcooling data for the inclination $\psi = 60°$ experiments show that the effect of subcooling is small in the early stages of the melting process. However, as the quasi-steady regime is reached the PCM with negligible initial subcooling clearly displays higher average Nusselt number behavior. Nusselt numbers 10–15% higher for no initial subcooling were also observed in melting heat transfer in a vertical cylinder [16].

A qualitative comparison can be made between the average Nusselt number enhancement due to heat source inclination in this study (see Fig. 8) and the enhancement found for pure natural convection (no phase change) in an inclined rectangular enclosure [17]. An increase of about 22% in $\overline{Nu}$ was found for $\psi = 60°$ over the vertical base case for $Pr = 0.7$, and a Rayleigh number based on cavity width $Ra = 4 \times 10^4$. However, very little enhancement was found for $\psi = 30°$. The present study (with phase change) shows an enhancement of about 32% in the $\psi = 60°$ case over the vertical base case for $Pr = 50$ and a Rayleigh number based on average melt gap of $Ra = 7 \times 10^6$. An enhancement of 9% was found for the $\psi = 30°$ data. Consistent with the above discrepancies, ref. [17] shows that $\overline{Nu}$ increases with Ra, providing at least a partial explanation for the higher values found here. Although a direct comparison cannot be made because of the difference in fluids, Rayleigh numbers and basic problem physics, it is instructive to see that the results for a natural-convection-driven inclined system with phase change are not entirely different from those of pure convection in an inclined enclosure. The reasonably good agreement between the one-dimensional model prediction and experimental data presented earlier also corroborate this statement.

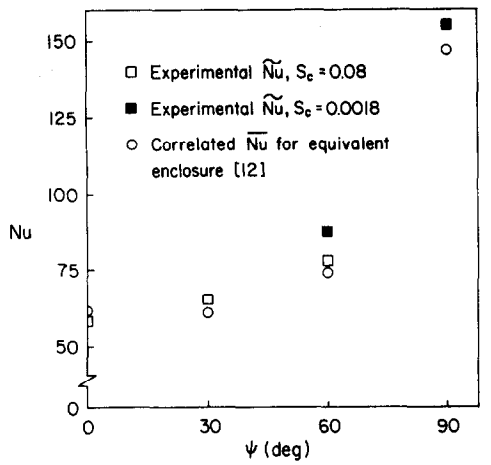

FIG. 9. Comparison of experimentally-determined average Nusselt number with correlations for natural convection in equivalent inclined enclosures in the absence of phase change.

A comparison is made in Fig. 9. of the average Nusselt number $\widetilde{Nu}$ determined experimentally in the quasi-steady melting regime ($\tau > 0.0025$), and the average Nusselt number $\overline{Nu}$ given by correlations [12] for rectangular enclosures as a function of the inclination angle. The average Nusselt number given by the published correlations is based on an equivalent rectangular enclosure of average width $\bar{s}$. The more rapid energy transport across the liquid layer due to three-dimensional natural convection at increasing ψ is evidenced by the higher Nusselt numbers. The values at $\psi = 90°$ are approx. 250% higher than those of the vertical heat exchanger orientation. The experimental values of $\widetilde{Nu}$ are generally higher than the $\overline{Nu}$ values calculated from published correlations, the one exception being the $\psi = 0°$ data. This may be attributed to the fact that as the PCM melts, the liquid contacts more of the heat exchanger wall than initially, increasing the wetted heat source area. As expected, the data for $S_c = 0.0018$ show even higher deviations, since no energy is expended in increasing the temperature of the solid. The results indicate generally that for small initial subcooling the overall heat transfer in quasi-steady melting can be approximated by correlations for rectangular enclosures without phase change given in the literature.

CONCLUSIONS

The experimental results of natural-convection-dominated inclined melting in a rectangular enclosure have been presented. The inclination produces a strong three-dimensional vortex motion that tends to Bénard convection patterns as the angle of inclination from the vertical is increased. Initial subcooling of the solid is found to promote the establishment of cellular motion. The three-dimensional natural convective motion provides more rapid energy transport to the solid–liquid interface than the two-dimensional boundary-layer recirculation found in melting from a vertical wall. This yields higher overall Nusselt numbers and, therefore, higher melting rates.

A one-dimensional model based on planar interface motion has been presented which employs heat transfer correlations for natural convection in inclined rectangular enclosures. The model predicts satisfactorily the melt fraction as a function of time. A correlation is presented detailing the effect of inclination angle on the timewise variation of the melt fraction.

Acknowledgements—One of the authors (B. W. Webb) acknowledges financial support of his graduate studies by an Eastman Kodak Company Graduate Fellowship. This work was supported, in part, by the Heat Transfer Program of the National Science Foundation under Grant No. MEA-8313573.

REFERENCES

1. R. Viskanta, Phase change heat transfer. In *Solar Heat Storage: Latent Heat Materials*, Vol. 1 (edited by G. A. Lane), pp. 153–222. Uniscience, CRC Press, Boca Raton, FL (1983).
2. N. W. Hale and R. Viskanta, Photographic observation of the solid–liquid interface motion during melting of a solid heated from an isothermal vertical wall, *Letters Heat Mass Transfer* **5**, 329–337 (1978).
3. E. M. Sparrow, R. R. Schmidt and J. W. Ramsey, Experiments on the role of natural convection in the melting of solids, *Trans. Am. Soc. mech. Engrs*, Series C, *J. Heat Transfer* **100**, 11–16 (1978).
4. R. Viskanta, Natural convection effects in phase change heat transfer. In *Natural Convection: Fundamentals and Applications* (edited by S. Kakac *et al.*), 845–877. Hemisphere, Washington, DC (1985).
5. L. A. Diaz and R. Viskanta, Visualization of the solid–liquid interface morphology formed by natural convection during melting of a solid from below, *Int. Commun. Heat Mass Transfer* **11**, 35–43 (1984).
6. M. Bareiss and H. Beer, Experimental investigation of melting heat transfer with regard to different geometric arrangements, *Int. Commun. Heat Mass Transfer* **11**, 323–333 (1984).
7. M. Okada, Analysis of heat transfer during melting from a vertical wall, *Int. J. Heat Mass Transfer* **27**, 2057–2066 (1984).
8. H. Ozoe, H. Sayama and S. W. Churchill, Natural convection patterns in a long, inclined rectangular box heated from below—Part I. Three-directional photographs, *Int. J. Heat Mass Transfer* **20**, 123–129 (1977).
9. H. Ozoe, K. Yamamoto, H. Sayama and S. W. Churchill, Natural convection patterns in a long inclined rectangular box heated from below—Part II. Three-dimensional numerical results, *Int. J. Heat Mass Transfer* **20**, 131–139 (1977).
10. A. Gadgil and D. Gobin, Analysis of two-dimensional melting in rectangular enclosures in presence of convection, *Trans. Am. Soc. mech. Engrs*, Series C, *J. Heat Transfer* **106**, 20–26 (1984).
11. C.-J. Ho and R. Viskanta, Heat transfer during melting from an isothermal vertical wall, *Trans. Am. Soc. mech. Engrs*, Series C, *J. Heat Transfer* **106**, 12–19 (1984).
12. I. Catton, Natural convection in enclosures. In *Heat Transfer—1978*, Vol. 6, pp. 13–30. Hemisphere, Washington, DC (1978).
13. R. H. Marshall, Natural convection effects in rectangular enclosures containing a phase change material. In *Thermal Storage and Heat Transfer in Solar Energy Systems* (edited by F. Kreith, R. Boehm, J. Mitchell and R. Bannerot), pp. 61–69. ASME, New York (1978).

14. E. M. Sparrow, S. V. Patankar and S. Ramadhyani, Analysis of melting in the presence of natural convection in the melt region, *Trans. Am. Soc. mech. Engrs*, Series C, *J. Heat Transfer* **99**, 520–526 (1977).
15. H. Rieger, V. Projahn, M. Bareiss and H. Beer, Heat transfer during melting inside a horizontal tube, *Trans. Am. Soc. mech. Engrs*, Series C, *J. Heat Transfer* **105**, 226–234 (1983).
16. R. G. Kemink and E. M. Sparrow, Heat transfer coefficients for melting about a vertical cylinder with or without subcooling and for open or closed containment, *Int. J. Heat Mass Transfer* **24**, 1699–1710 (1981).
17. H. Ozoe, H. Sayama and S. W. Churchill, Natural convection in an inclined rectangular channel at various aspect ratios and angles—experimental measurements, *Int. J. Heat Mass Transfer* **18**, 1425–1431 (1975).

TRANSFERT THERMIQUE LORS D'UNE FUSION DOMINEE PAR LA CONVECTION NATURELLE DANS UNE ENCEINTE RECTANGULAIRE INCLINEE

Résumé—On étudie expérimentalement le transfert thermique à la fusion dans une enceinte rectangulaire inclinée. L'effet de l'inclinaison est d'établir un mouvement tridimensionnel de convection naturelle qui s'intensifie lorsque l'angle d'inclinaison à partir de la verticale est augmenté. La tridimensionnalité du champ d'écoulement provoque une fusion non uniforme du solide. La morphologie de l'interface est utilisée pour inférer la structure de l'écoulement et le transfert tridimensionnel d'énergie. Ces configurations d'écoulement sont trouvées dépendantes de l'angle d'inclinaison et du sous-refroidissement initial du solide. Une formule est présentée pour décrire l'effet de l'inclinaison sur la variation dans le temps de la fraction fondue. Un modèle théorique monodimensionnel est donné et les prévisions sont comparées à des données expérimentales.

WÄRMEÜBERTRAGUNG BEIM SCHMELZEN BEI FREIER KONVEKTION IN EINEM GENEIGTEN RECHTECKIGEN HOHLRAUM

Zusammenfassung—Die Wärmeübertragung beim Schmelzen in einem geneigten rechteckigen Hohlraum wurde experimentell untersucht. Unter dem Einfluß der Neigung bildet sich infolge freier Konvektion eine dreidimensionale Strömung aus, deren Intensität bei Vergrößerung des Winkels gegenüber der Senkrechten zunimmt. Wegen des dreidimensionalen Strömungsfeldes erfolgt das Schmelzen der festen Phase nicht einheitlich. Aus der Form der Schmelzfront ergeben sich Rückschlüsse auf die Strömungsform und auf den dreidimensionalen Wärmetransport. Es wurde herausgefunden, daß diese Strömungsformen vom Neigungswinkel und von der Anfangsunterkühlung abhängig sind. Eine Beziehung wird vorgestellt, die den Einfluß des Neigungswinkels auf die zeitliche Änderung der geschmolzenen Phase beschreibt. Ein theoretisches eindimensionales Modell wurde aufgestellt; die berechneten Ergebnisse wurden mit Versuchsdaten verglichen.

ТЕПЛОПЕРЕНОС С ПРЕОБЛАДАЮЩЕЙ ЕСТЕСТВЕННОЙ КОНВЕКЦИЕЙ ПРИ ПЛАВЛЕНИИ В НАКЛОННОЙ ПРЯМОУГОЛЬНОЙ ПОЛОСТИ

Аннотация—Экспериментально исследуется теплоперенос при плавлении в наклонной прямоугольной полости. Полость наклонена с целью получения трехмерного естественноконвективного движения, которое усиливается с увеличением угла отклонения от вертикали. Трехмерность поля течения приводит к неравномерному плавлению твердой фазы. Строение границы используется для нахождения структуры течения и степени трехмерности переноса энергии. Найдено, что структура течения зависит от угла наклона и начального недогрева твердого тела. Представлена зависимость, описывающая влияние величины угла наклона на временное изменение доли расплавленной фазы. В общих чертах описана одномерная теоретическая модель, и результаты анализа сравниваются с данными экспериментов.